

Original Research

Construction of enzalutamide-resistant cell model of prostate cancer and preliminary screening of potential drug-resistant genes

Tao Feng* , Dechao Wei*, Jiahui Zhao, Qiankun Li, Pengju Guo, Xiaobing Yang, Mingchuan Li, Yongguang Jiang and Yong Luo

Department of Urology, Beijing Anzhen hospital, Capital Medical University, Beijing 100029, China

Corresponding author: Yong Luo. Email: luoyonganzhen@163.com

*These authors contributed equally to this work.

Impact statement

As far as PCa patients are concerned, among different factors in causing their death, CRPC held a large proportion. For the moment, enzalutamide is a therapeutic drug to CRPC, second to none in efficacy, whereas enzalutamide-resistance blocks the treatment of CRPC patients with it to a great extent. Therefore, it had always become one of the goals in CRPC treatments. In our study, we established an enzalutamide-resistant cell model and verified its drug resistance. Furthermore, we also screened some functional resistance genes involved in developing enzalutamide-resistance and small molecular drugs concerned with the amelioration of enzalutamide-resistance. Of clinical relevance, EGR1 could represent a novel diagnostic marker for enzalutamide-resistant CRPC, and through targeting EGR1, enzalutamide-resistant CRPC sufferers may be treated.

Abstract

Among many factors of causing castration-resistant prostate cancer (CRPC) progression, a growing number of evidences have shown androgen receptors play a critical role. Therefore, blocking androgen receptor remains a therapeutic goal of CRPC. However, resistance to androgen receptor inhibitors, for example, enzalutamide, limits therapeutic efficacy for many patients. In this study, to develop an enzalutamide-resistant cell model for molecular mechanism investigation of enzalutamide-resistance, we continuously treated C4-2B cells with multiplied concentrations of enzalutamide. The IC₅₀ of resistant cells was identified as 14.7705 μ M, and the resistance index was calculated as 12.4. In addition, we verified the resistance of resistant cells through experiments *in vivo* and found the genes in androgen receptor signaling pathway (androgen receptor, Jagged1, Notch1) and those in androgen receptor alternative signaling pathways behaved the opposite. For some of the former, their mRNA and protein expression reduced markedly while for the latter, for example, CXCR7, AKT, STAT3, FOXP3, they rose dramatically in the expression level of protein and mRNA. More importantly, the tumor volume, tumor wet weight, PSA and VEGF secretion level, positive staining rate of Ki67 nuclei in resistant strain heterogeneous tumor treated with enzalutamide were significantly higher than those of maternal cell heterogeneous tumor treated with enzalutamide, whereas no obvious difference was detected between resistant strain heterogeneous tumor treated with enzalutamide and those of the resistant strain treated with reference drug. Finally, we identified 654 differentially expression genes and 2 compounds (atracurium besilate, methotrexates) associated with the amelioration of enzalutamide-resistance. Overall, we successfully established an enzalutamide-resistance cell model and screened out some resistance genes and candidate small molecule drugs.

neous tumor treated with enzalutamide, whereas no obvious difference was detected between resistant strain heterogeneous tumor treated with enzalutamide and those of the resistant strain treated with reference drug. Finally, we identified 654 differentially expression genes and 2 compounds (atracurium besilate, methotrexates) associated with the amelioration of enzalutamide-resistance. Overall, we successfully established an enzalutamide-resistance cell model and screened out some resistance genes and candidate small molecule drugs.

Keywords: Castration-resistant prostate cancer, enzalutamide, endocrine resistance, CXCR7, FOXP3, bioinformatics

Experimental Biology and Medicine 2021; 246: 1776–1787. DOI: 10.1177/15353702211012625

Introduction

In the world, as far as the male is concerned, among different factors of causing their death, prostate cancer (PCa) held a large proportion which is malignancy and not strange at all to people.¹ In 1941, in term of PCa treatments,

second to castration, Huggins and Hodges made some major founding, which makes androgen deprivation therapy (ADT) preference thereafter.² Unfortunately, above treatments still have some limitations and majority of PCa sufferers will eventually progress to develop CRPC after

two to three years of receiving ADT.³ Over the past few decades, there are no other effective measures other than docetaxel chemotherapy, which can barely benefit the survival of patients with CRPC⁴.

Enzalutamide renovated the endocrine therapy concept of CRPC by blocking nuclear translocation and interaction with co-activators, and more importantly, the median survival time (MST) of CRPC has been prolonged considerably.⁴ According to the currently existing literatures, no matter for the CRPC patients who failed chemotherapy,⁵ or for those having received chemotherapy-naïve,⁶ enzalutamide can all reduce their death rate. However, with the vast application of enzalutamide, new issues and challenge have arisen: (1) About 42% of CRPC patients are insensitive to enzalutamide.⁷ (2) Although some patients are sensitive to initial treatment of enzalutamide, resistance problem still appeared after 11.2 months,⁸ acquired resistance to enzalutamide is universal over time. Nevertheless, the underlying mechanisms of enzalutamide resistance remain largely unclear. Hence, it seems very critical to make clear of them as much as possible so that CRPC outcomes can be further improved.

This study reports our novel approach to construct an enzalutamide-resistant cell model, which provides a good foundation for research on resistant mechanism. Furthermore, we also preliminarily screened some enzalutamide resistance genes and candidate molecular drugs, which may become the potential therapeutic target of CRPC.

Materials and methods

Cell lines and reagents

Human PCa cell lines (C4-2B cells) and reagents (Enzalutamide): the former was free, provided by Dr Timothy Thompson (MD Anderson Cancer Center) while the latter purchased from Selleck Chemicals (Selleck, USA). At room temperature, prepare a RPMI medium in a humidified incubator containing 5%CO₂ with streptomycin, fetal calf serum (FBS) and penicillin which is 100 µg/mL, 10% and 100 U/mL, respectively, in concentration.

Cell viability assay

The MTT assay aimed to identify the initial concentration of enzalutamide for subsequent experiment. We seeded C4-2B cells in a 96-well plate at 5×10^3 cells/well and incubated these for 24 h in 37°C with 5%CO₂. Then we treated the cells with enzalutamide in various concentrations (0, 0.5, 1, 1.5, 2, 2.5 µM) and incubated the cells a further 24 h. Meanwhile, we added 10 µL MTT. The plate was centrifuged after 4 h of incubation, with supernatant discarded afterwards and 150 µL DMSO added into its wells, respectively. By microplate reader (FlexStation 3, Molecular Devices, USA), we could get to know the absorbance of each well. After that, the initial treatment concentration of enzalutamide was determined by IC50 value according to the MTT curve.

Screening of C4-2B resistant cell lines

C4-2B cells in the logarithmic phase were vaccinated in 6-well culture plate and the initial concentration of enzalutamide was added when cell confluency reached 30%. The culture medium was replaced after 24 h, and enzalutamide was added again when the cell-density reached 70%. After further 24 h, the medium was changed and then subcultured or harvested for cryopreservation when cell confluency reached 90%. The concentration of enzalutamide was doubled every four weeks (2.5 µM and 5 µM).

Oxidative DNA damage assay

To evaluate oxidative DNA damage level of resistant-cells, 8-OHdG was measured by ELISA using the ELISA kit for 8-OHdG (Abcam, Cambridge, MA, USA). Briefly, the cells (1.5×10^4 cells/well) were placed into 96-well plates. Then 50 µL sample or standard were added to each well and were detected by 8-OHdG antibody. Optical densities were determined at 450 nm using a microplate reader according to manufacturer's instructions. Finally, we assessed cell DNA integrity by calculating the concentration of 8-OHdG based on a standard curve. When the DNA integrity of enzalutamide-resistant cell line was similar to parental cell lines (C4-2B), this cell line was carried out for subsequent experiments due to its lower damage.

Determination of enzalutamide resistance level

We seeded C4-2B in 96-well plates at 5×10^3 cells/well, respectively, and added cell suspension at 100 µL/well at the same time. After an incubation of cells overnight at room temperature under saturated humidity atmosphere containing 5%CO₂. After that, different concentrations of enzalutamide (0, 1, 2, 5, 7.5, 10, 15, 20, 30, 40, 50, 75, 100 µM) were added to cells. We also added 10 µL MTT reagent after further 24 h of incubation. The supernatant was discarded following 4-h incubation. Finally, the resistance index (RI) was calculated by the absorbance in a microplate reader. $RI = IC_{50}(\text{resistant cell}) / IC_{50}(\text{parental cells})$, resistant criterion (RI: <5, low resistance; 5~15, moderate resistance; >15, high resistance).

Quantitative real-time polymerase chain reaction

To determine the concentration and purity of RNA, with the Trizol reagent, we extracted RNA from the cells totally. Then QRT-PCR was carried out: firstly, the RNA was denatured twice under high temperature (95°C) successively, one time for 10 min and the second time for 40 cycles, 30 s/cycle continuously; secondly, the RNA was provided a 30-s annealing at 60°C. Each sample was assayed in triplicate and all quantifications were normalized against endogenous GAPDH reference. The relative expression of target genes was quantified using $2^{-\Delta\Delta Ct}$ method. Primers used are as follows: AR (forward:5'-CCAGGGACCATGTTTTGCC-3'; reverse: CCAGGGACCATGTTTTGCC-3'), Jagged1(forward:5'-ATGCAGAACGTG AATGGAGAG-3'; reverse:5'-GCGGGACTGATACTCCTTGAG-3'), Notch1 (forward: 5'-GAGGCGTGGCAGACTATGC-3'; reverse: 5'-CTTGACTCCGTCAGCGTGA-3'), CXCR7(forward:5'-TC

TGCGTCCAACAATGAG-3'; reverse: 5'-AGGAAGTAG A AGACAGCGATA-3'), AKT (forward: 5'-GTCGCCTGCCC TTCTACAAC-3'; reverse: 5'-CCACACGATACCGGCAA AGA-3'), STAT3 (forward: 5'-CAGCAGCTTGACACA CGG TA-3'; reverse: 5'-AAACACCAAAGTGGCATGTGA-3'), FOXP3 (forward: 5'-CATTCCCAGAGTTCCTCCACA-3'; reverse: 5'-CATTGAGTGTCCGCTGCTTC-3'), GAPDH (forward: 5'-TCAAGAAGGTGGTGAAGCAGG-3'; reverse: 5'-TCAAAGGT GGAGGAGTGGGT-3')

Western blotting analysis

The cells cultured in 6-well plates were placed on ice and lysed with lysate buffer supplemented with PMSF (120 μ L) 30 min. The supernatant was collected as total cellular protein the concentration of which can be determined with the descriptions on BCA Protein Assay Kit, followed after centrifugation at 12,000 r/min for 300 s at 4°C. By protein concentration, 40 μ g/load protein was clarified. In the following, firstly, we prepared nitrocellulose membranes and blocked them into 5% non-fat dry milk for 120 min, secondly, incubated them: AR (1:500, Santa Cruz Biotechnology, Danvers, MA, USA), Jagged1 (1:500, Abcam, Cambridge, MA, USA), Notch1 (1:1000, Santa Cruz Biotechnology, Santa Cruz, CA, USA), AKT (1:1000, Cell Signaling Technology, Danvers, MA, USA), STAT3 (1:1000, Abcam, Cambridge, MA, USA), CXCR7 (1:500, Abcam, Cambridge, MA, USA), FOXP3 (1:200, Abcam, Cambridge, MA, USA), GAPDH (1:1000, Cell Signaling Technology, Danvers, MA, USA) overnight at the temperature of 4°C, and thirdly we separated the clarified protein on 8~12% SDS-PAGE gels with an electro-transfer onto these membranes which later received another 120-min incubation with horseradish peroxidase (HRP)-conjugated secondary antibody (1:50,000, all from Wuhan Boster Biological Technology) after being washed with PBS. With ECL, color development was performed. Finally, the protein band was evaluated by Image J software in grayscale and the relative protein expression calculated against the grayscale of GAPDH.

Animal study

Nude mice (male, 28 days old, 20–25 g) were purchased from Charles River Laboratories (Boston, MA, USA). The approval of experiments on animals was gained from the Committee on the Ethics of Animal Experiments of the Capital Medical University, Beijing, China. The experiment ended with animal euthanasia. Suspensions of cells (1×10^6 cells in a volume of 1 mL of RPMI 1640) were subcutaneously implanted into castrated nude mice. The castrated nude mice were randomly divided into three groups: C + E group, CE + V group, and CE + E group. In the study, at least 10 mice in each group were selected the tumor size of which was monitored weekly and measured by caliper measurements based on the expression: length \times width²/2. When the size of tumor became 30 and 50 mm³, treatments started: implanting the mice in the first group C4-2B and treating them with enzalutamide (10 mg/kg, oral gavage, daily); implanting the mice in the second group C4-2B-ENZ and treating them with vehicle control for enzalutamide (1% carboxymethyl cellulose, 0.1% Tween-80, 5% DMSO

in water, oral gavage, daily); at last, implanting the mice in the third group C4-2B-ENZ and treating them with enzalutamide (the taking way is similar to the first group).

Immunohistochemical analysis

After all the tumors of mice were obtained at the endpoint of animal protocol, they were wrapped into paraffin wax finally through treatment with 4% paraformaldehyde, dehydration with ethanol, and a washing with xylene. Through the formalin fixation of paraffin wax, Ki67 immunohistochemistry was performed. Subsequently, the sectioned slides were incubated by anti-Ki67 antibodies (1:300, Santa Cruz Biotechnology) at 4°C overnight, and then a HRP polymer-conjugated secondary antibody (1:300, Dako, Glostrup, Denmark) for 2 h. With DAB/H₂O₂, we could observe the immunoreactions the particularity of which could be also verified by substituting the primary antibody with PBS. Finally, based on an image analysis system (Eclipse 90i; Nikon Instrument Inc., Tokyo, Japan), we selected 10 high-power fields at random, and with the Nikon NIS-Elements version 3.0 software, we counted the numbers of positively stained cells and calculated the percentage of positive cells.

VEGF and PSA ELISA

The following three experiments were carried out with mutual noninterference. (1) Venous blood (1 mL) was collected by orbital blood collection and centrifuged to get serum. The instructions on ELISA (R&D systems) were the base of the following two ones: (2) with VEGF ELISA, VEGF levels were quantified; (3) with PSA ELISA, PSA levels were quantified.

Screening of enzalutamide resistance genes

In addition to transcriptome sequencing, the other two terms were also conducted by Yiming Fuxing Biotechnology Corporation (Beijing, China): RNA library construction and total RNA extraction. All data were subjected to quality control, background correction, and logarithmic conversion using R software 3.6.1. Differentially expressed genes (DEGs) between C4-2B-ENZ cells and C4-2B cells were identified with a threshold of $P < 0.05$ and $|\log_{2}FC| > 1.5$ by using the R package "limma". To get a more understanding of the biological functions of enzalutamide resistance, after carrying out gene set enrichment analysis (GSEA), we also conducted PPI network analysis by virtue of STRING database. Finally, according to scores from high to low, we identified the top 10 genes as hub ones by Cytoscape plug-in cytoHubba.

Identification of potentially small molecules

To explore potential drugs that may ameliorate enzalutamide-resistance, we processed DEGs via CMAP analysis (<https://portals.broadinstitute.org/cmap>), which integrated diseases, drugs, genes based on gene expression profiles.^{9,10} Subsequently, the enrichment score of each molecule drug was calculated, which ranged from -1 to 1. In the current study, positive mean represented that

Table 1. Hub genes based on PPI analysis.

Rank	Symbol	Score	Expression	logFC	P-value
1	FOS	21	Up-regulated	1.582	2.21E-06
2	MYC	21	Down-regulated	-2.435	8.20E-08
3	C3	18	Up-regulated	1.537	8.95E-06
4	APOE	13	Up-regulated	2.26	1.55E-06
5	EGR1	12	Up-regulated	3.502	1.68E-07
6	CYR61	11	Up-regulated	1.626	2.96E-08
7	IGFBP5	11	Up-regulated	2.474	1.78E-07
8	CTGF	11	Up-regulated	1.813	2.08E-08
9	SYP	10	Down-regulated	-1.829	1.22E-04
10	COL3A1	9	Up-regulated	2	1.16E-08

these selected drugs may share similar functions with enzalutamide. In contrast, negative mean indicated that enzalutamide and these drugs combination treatment may be able to solve enzalutamide-resistance. We herein screened compounds by setting the criteria as P value < 0.05 .

Molecular docking

To further investigate the association between small molecules and hub genes, molecular docking calculations were done using AutoDock Vina. Here, we chose EGR1, which the highest up-regulation fold in Table 1, to perform

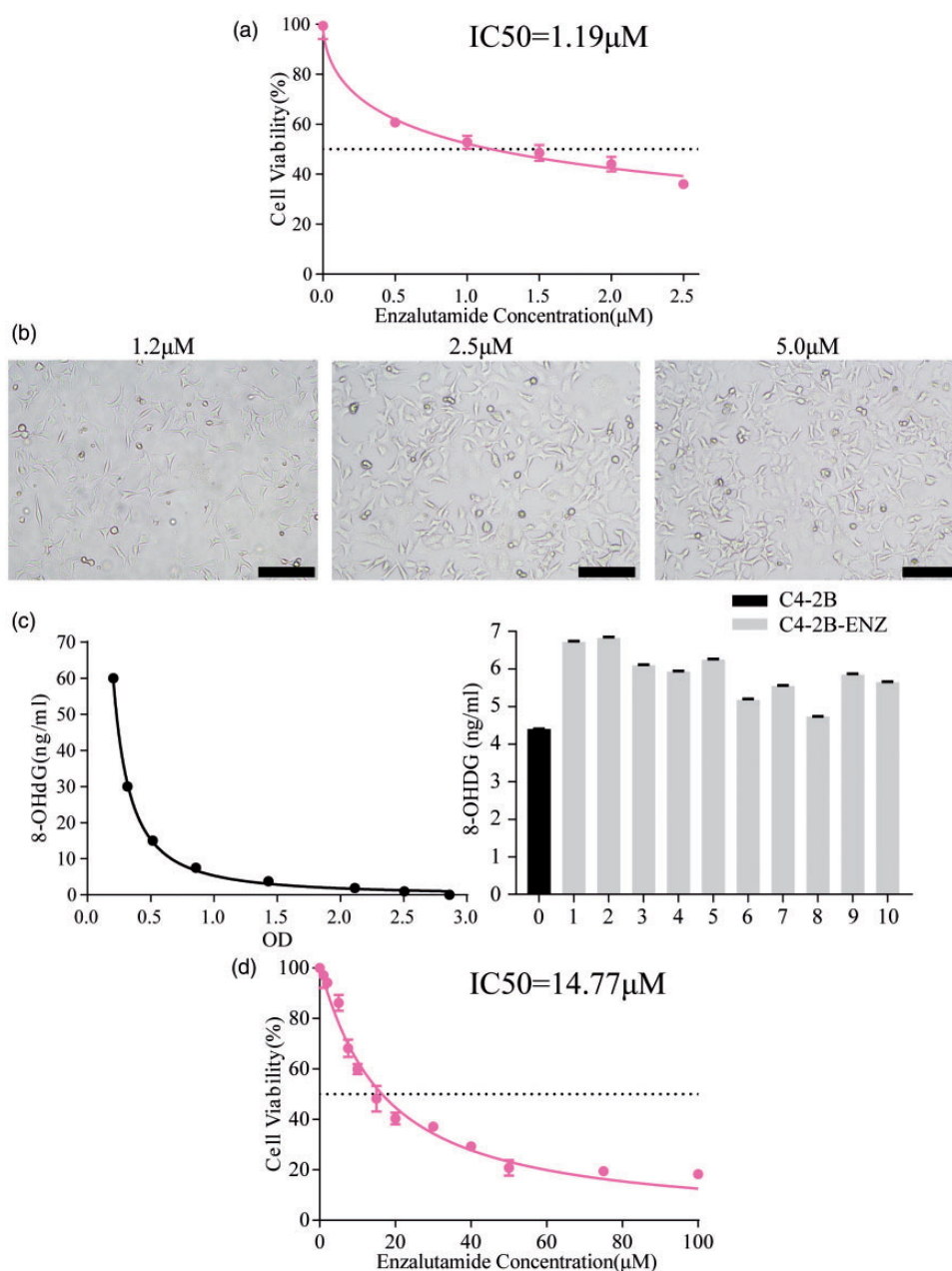


Figure 1. Establishment of enzalutamide-resistant cell model. (a) IC₅₀ curve was used to determine the initial treatment concentration of enzalutamide. (b) Morphologic changes in C4-2B cells treated under different concentrations. Scale = 400 μM. (c) 8-OHdG levels in resistant cells were detected using ELISA. (d) Enzalutamide-resistance level was identified by IC₅₀ curve in resistant cells using MTT assay. All data were the mean \pm SE of three separate measurements done in triplicate. (A color version of this figure is available in the online journal.)

molecular docking with top 10 compounds in CMAP analysis. The three-dimensional structures of EGRI, provided by RCSB Protein Data Bank, for all compounds were downloaded from PubChem database with MOL2 format. Following the docking studies, the binding energy and combination type were displayed, with the least binding energy and hydrogen bonds were considered to have the best docked pose. Finally, the binding mode between compounds and EGR1 was visualized by Pymol 2.1 software.

Statistical analysis

In the experiment, all the data obtained were an average and there would be a statistical difference to a great extent if P -values < 0.05 . In addition, analysis of the data obtained in this experiment was conducted based on Student's t -test and statistically on SPSS 25.0 software for Windows (SPSS Inc., Chicago, IL, USA).

Results

Establishment of enzalutamide resistance cell model

The initial treatment concentration of enzalutamide was defined as $1.2 \mu\text{M}$ by MTT assay (Figure 1(a)). After that,

C4-2B cells received treatment continuously with enzalutamide at different concentrations ($1.2 \mu\text{M}$, $2.5 \mu\text{M}$, and $5 \mu\text{M}$). We found that cells displayed a more vacuoles with increased concentration of enzalutamide (Figure 1(b)). To assess levels of oxidative DNA damage, 10 C4-2B-ENZ cells at $5 \mu\text{M}$ concentration were measured. No significant differences in 8-OHdG were noted in the eighth cell line and parent cell line, but elevated 8-OHdG concentrations was found in other nine cell lines, which means these cell lines both have different degrees of DNA damage after enzalutamide treatment (Figure 1(c)). Finally, IC₅₀ value of the 8th cell lines was measured as $14.77 \mu\text{M}$ and the RI was calculated as 12.4, which belongs to moderately enzalutamide-resistant cell line (Snow resistant criterion) (Figure 1(d)). Thus, the cell line was utilized in subsequent experiments.

Validation of resistance cell lines in vitro experiments

To determine resistance of C4-2B-ENZ cells, we carried out a series of *in vitro* experiments. We have demonstrated that four genes were closely associated with enzalutamide-resistance in our previous study.¹¹ Here, through qPCR and Western blot analysis, the expression levels of these four genes and some AR signaling pathway genes were

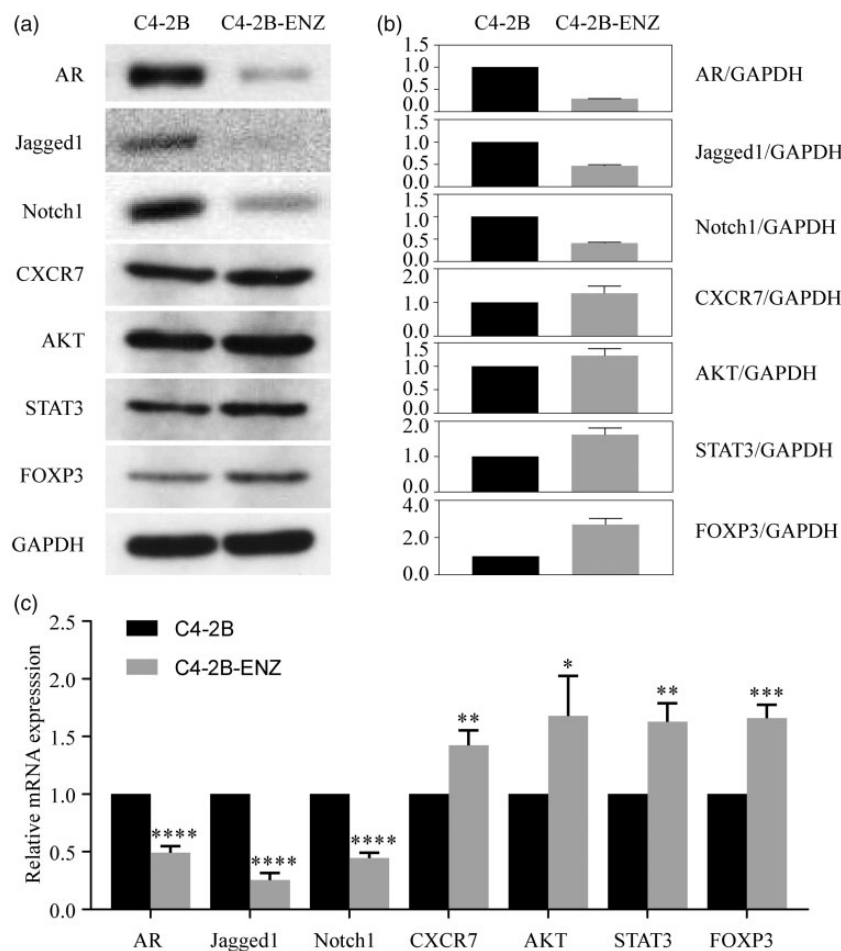


Figure 2. The resistance of resistant cells was verified *in vitro* experiments. (a–c) In terms of AR, Jagged1, Notch1, CXCR7, AKT, STAT3 and FOXP3 proteins in C4-2B cells and C4-2B-ENZ cells, analysis of the protein level and the mRNA level was carried out respectively by Western blotting and QRT-PCR, while the quantified ratio of the protein band intensity normalized to GAPDH. The experimental data obtained in this paper were all the mean \pm SE of three separate measurements done in triplicate. * $P < 0.05$, ** $P < 0.01$, *** $P < 0.001$, **** $P < 0.0001$.

further validated. In addition, the C4-2B-ENZ samples were superior to the C4-2B ones in mRNA and protein expression of CXCR7, AKT, STAT3, FOXP3 was also corroborated. Conversely, the mRNA and protein expression levels of AR signaling pathway genes (AR, Jagged1, Notch1) in C4-2B-ENZ samples were lower than C4-2B samples (Figure 2(a) to (c)). These results revealed that AR signaling pathway was dramatically suppressed and CXCR7 signaling pathway was significantly elevated in C4-2B-ENZ cells.

Validation of resistance cell lines in vivo experiments

As for the resistance of C4-2B-ENZ cells, we also performed sets of experiments *in vivo*. Animals were treated according

to the scheme illustrated in Figure 3(a). Tumors in the CE+E group grew significantly rapidly ($P=0.0296$) as well as their tumor wet weight ($P<0.0001$) compared with the C+E group, but there were no obvious differences compared to CE+V group (tumor size, $P=0.569$; tumor wet weight, $P=0.707$) (Figure 3(b) to (d)). Meanwhile, higher VEGF and PSA levels were in the CE+E group by comparing to the C+E group (VEGF: $P=0.0003$ and PSA: $P<0.0001$), whereas compared to the CE+V group, the CE+E group still did not behave different statistically (VEGF: $P=0.158$ and PSA: 0.055) (Figure 3(e) and (f)). Through immunohistochemistry, we obtained that among the three groups: the CE+E group, the C+E group, and the CE+V group, the first one was superior to the second one

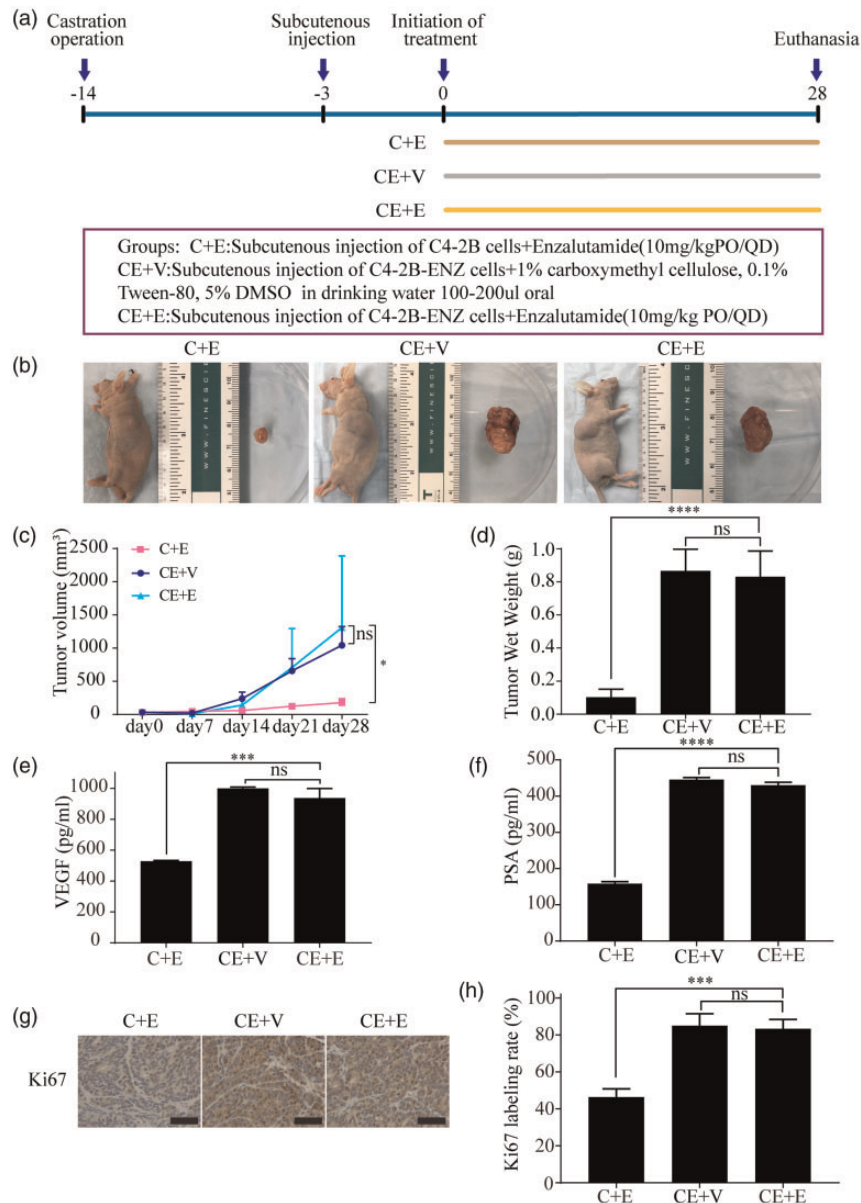


Figure 3. The resistance of resistant cells was verified *in vivo* experiments. (a) The protocol of experimental design and animal groups. (b–d) Significant difference in volumes and wet weights of tumor xenografts under different groups. (e–f) The secretion of VEGF and PSA in three groups was determined by VEGF-ELISA and PSA-ELISA. (g–h) Immunohistochemical staining was used for Ki67 detection in expression in three different experimental groups for evaluating the histological characteristics. Scale = 400 μ M. The experimental data in this paper were all the mean \pm SE or rate of three separate assays done in triplicate. (A color version of this figure is available in the online journal.)

($P = 0.0007$), while there was almost no difference between the first one and the last one ($P = 0.746$) (Figure 3(g) and (h)) in term of Ki67 expression. Taking together, these results indicated that C4-2B-ENZ have developed resistance towards enzalutamide.

Screening of associated ENZ-resistance genes by bioinformatics

Transcriptome sequencing between C4-2B cells and C4-2B-ENZ cells was conducted so as to verify the positive role of gene activities in resisting enzalutamide. Based on the results of differential expression analysis, identification was provided for a total of 654 regulated DEGs: 211 up and 443 down largely (Figure 4(a) and (b)). According to GSEA results, we found these common DEGs were most significantly enriched in angiogenesis and NF- κ B signaling pathways; however, the oxidative phosphorylation and DNA repair pathways were significantly suppressed (Figure 5(a) and (b)). In this regard, this could be due to some reasons. Abnormal hyperplasia of tumor vessels, activation of AR and AR-Vs through NF- κ B signaling pathways during the course of enzalutamide-resistance. Meanwhile, the formation of classical metabolic adaptation by virtue of a core metabolic switch forms oxidative

phosphorylation to glycolysis during enzalutamide-resistance. Another interpretation is that inhibition of DNA repair disrupts the genome stability leading to enhanced mutation frequency of some genes in AR signaling pathway. Subsequently, DEGs were performed to PPI analysis based on the STRING online database and Cytoscape software (<http://cytoscape.org/>) (Figure 6). The top 10 hub genes identified by cytoHubba are listed in Table1.

CMAF analysis and molecular docking

According to the analysis DEGs between C4-2B-ENZ samples and C4-2B samples, identification of 10 small molecule drugs correlated closely, see Table 2, to a great extent was carried out. Thereinto, ceforanide, lycorine, methotrexate, atracurium besilate, and pregnenolone were correlated negatively with the potential to reverse the status of enzalutamide-resistance. Subsequently, these 10 compounds filtered by CMAF analysis were docked with EGR1 to obtain docking result (Table 3). We found all compounds showed a high binding affinity against the target protein due to their binding energy less than -5 kcal/mol. Obviously, there were relatively higher binding affinity between methotrexate and atracurium besilate and EGR1

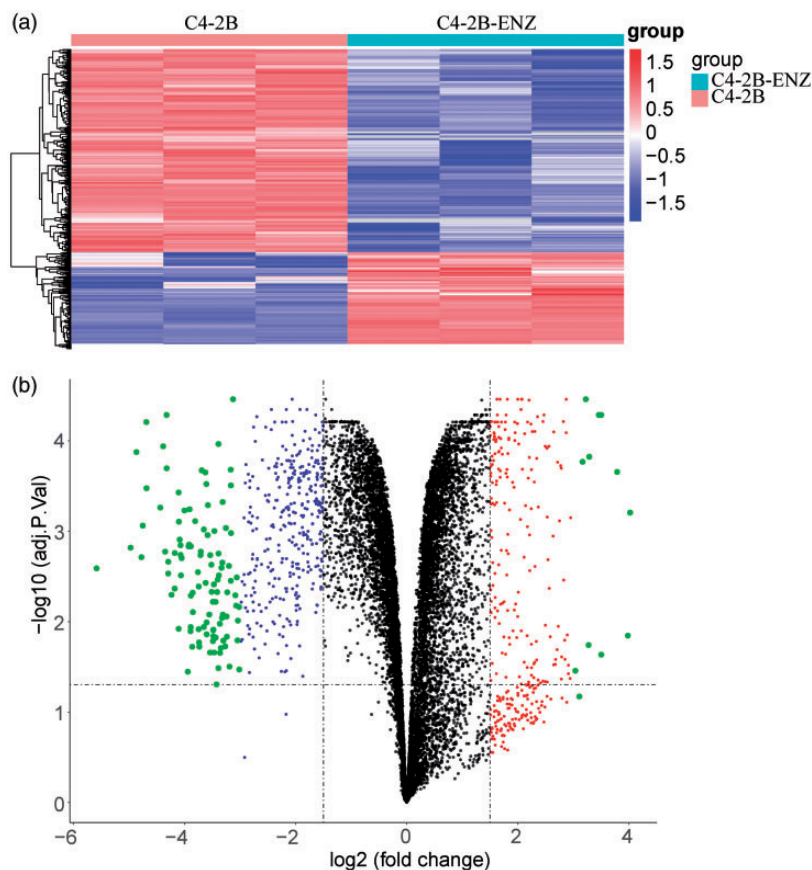


Figure 4. Differentially expressed genes (DEGs) between C4-2B cells and C4-2B-ENZ cells in our transcriptome sequencing data. (a) Heatmap displayed hierarchical clustering of DEGs ($n = 654$). Red and blue represented different levels of gene expression respectively, the former upward while the latter downward. (b) Volcano plot showed DEGs between C4-2B and C4-2B-ENZ cells. X-axis represented \log_2 fold change and Y-axis represented $-\log_{10}$ (adjusted P -value). Black dots represented upregulated genes or downregulated genes defined as $|\log_{FC}| < 1.5$ and adjusted $P < 0.05$. Red dots represented upregulated genes defined as $1.5 < \log_{FC} < 3$ and adjusted $P < 0.05$. Blue dots represented downregulated genes defined as $-1.5 < \log_{FC} < -3$ and adjusted $P < 0.05$. Green dots represented upregulated genes or downregulated genes defined as $|\log_{FC}| > 3$ and $P < 0.05$. (A color version of this figure is available in the online journal.)

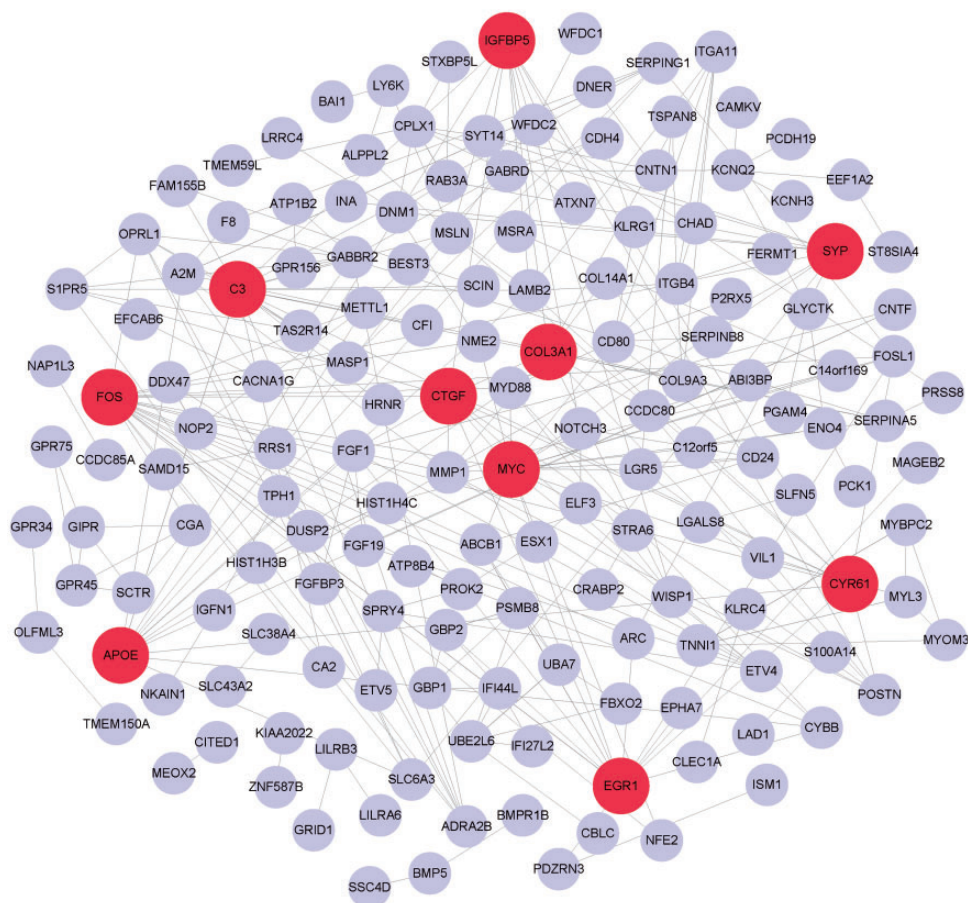


Figure 5. The PPI analysis. A total of 654 DEGs (211 up-regulated genes and 443 down-regulated genes) were filtered into the PPI network. Red nodes suggested top 10 hub genes with the highest scores. Lines reflected the interactions between these genes. (A color version of this figure is available in the online journal.)

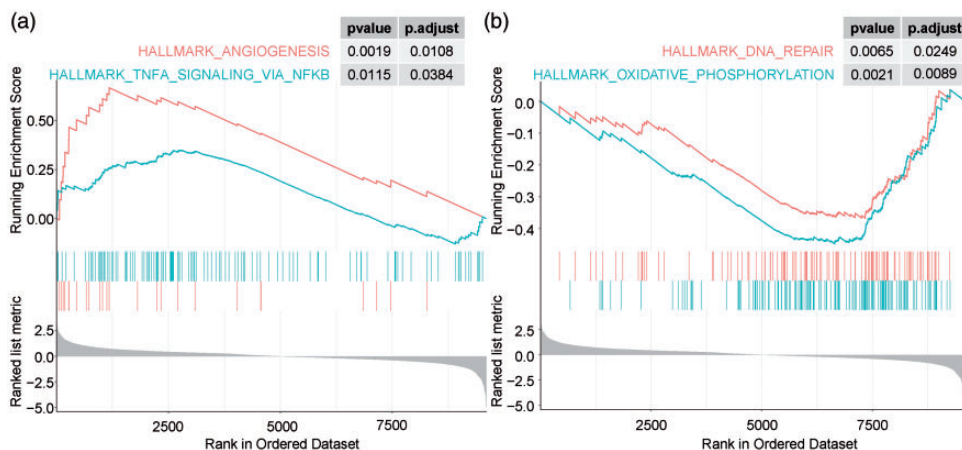


Figure 6. Gene set enrichment analysis (GSEA) analysis of 654 DEGs. (a–b) Here, through gene permutation, the P value of the gene sets taken from “hallmark gene sets” was worked out. The results revealed that the DEGs were mainly enriched in angiogenesis and TNFA signaling via NF- κ B related pathways, whereas negatively correlated with DNA repair and oxidative phosphorylation pathways. (A color version of this figure is available in the online journal.)

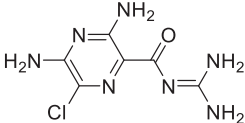
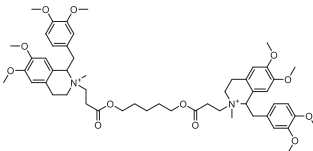
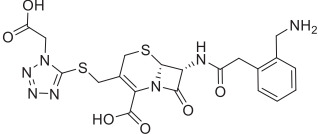
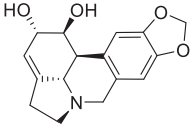
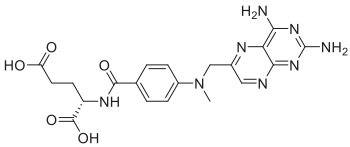
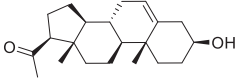
compared with other eight compounds. Meanwhile, 3D structure of EGR1-atracurium besilate complex and EGR1-methotrexate complex is displayed in Figure 7(a) and (b). In EGR1-atracurium besilate complex, the methoxy groups and carbonyl oxygen atoms form hydrogen bond with activity groups of amino acid, which mean atracurium besilate was able to match well with EGR1 protein.

Similarly, the amino group and the carboxyl group of methotrexates can form hydrogen bonds to the activity group on multiple residues of amino acid, which mean methotrexate can form a stable complex with EGR1 protein. Hence, these two compounds were both considered as potential EGR1 inhibitor, which may reverse the status of enzalutamide-resistance.

Table 2. CMAP analysis.

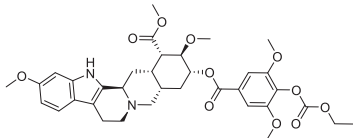
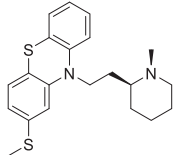
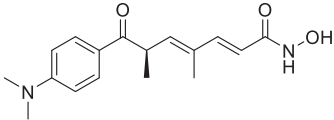
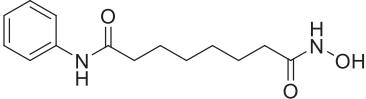
Rank	cmap name	Mean	n	Enrichment	P	Specificity
1	Trichostatin A	0.5	92	0.584	0	0.3175
2	Ceforanide	-0.88	2	-0.997	0.00004	0
3	Lycorine	-0.739	3	-0.952	0.00022	0.0126
4	Methotrexate	-0.797	2	-0.985	0.0005	0
5	Syrosingopine	0.785	2	0.977	0.00087	0.005
6	Amiloride	0.802	2	0.972	0.00133	0
7	Atracurium besilate	-0.771	2	-0.974	0.00139	0
8	Thioridazine	0.42	11	0.542	0.0015	0.2326
9	Pregnenolone	-0.782	2	-0.973	0.00151	0.0075
10	Vorinostat	0.545	7	0.65	0.00192	0.488

Table 3. Molecular docking results.

Name	Target	Compound structure	Binding energy (kcal/mol)	Combination type
Amiloride	EGR1		-5.05	Hydrogen bonds, hydrophobic interactive
Atracurium besylate	EGR1		-9.54	Hydrogen bonds, hydrophobic interactive, π - π stacking
Ceforanide	EGR1		-7.56	Hydrogen bonds, hydrophobic interactive, π - π stacking
Lycorine	EGR1		-5.29	Hydrogen bonds, hydrophobic interactive, π - π stacking
Methotrexate	EGR1		-8.54	Hydrogen bonds, hydrophobic interactive, π - π stacking
Pregnenolone	EGR1		-5.48	Hydrogen bonds, hydrophobic interactive

(continued)

Table 3. Continued.

Name	Target	Compound structure	Binding energy (kcal/mol)	Combination type
Syrosingopine	EGR1		-8.41	Hydrogen bonds, hydrophobic interactive, π - π stacking
Thioridazine	EGR1		-6.81	Hydrogen bonds, hydrophobic interactive, π - π stacking
Trichostatin A	EGR1		-6.52	Hydrogen bonds, hydrophobic interactive
Vorinostat	EGR1		-6.49	Hydrogen bonds, hydrophobic interactive

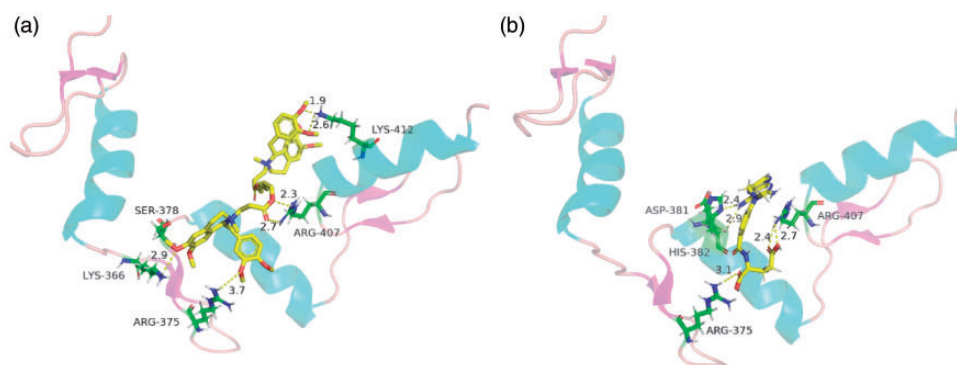


Figure 7. 3D structure of EGR1-atracurium besilate complex and EGR1-methotrexate complex based on molecular docking. (a) The binding mode of atracurium besilate to the EGR1 was analyzed, in which active amino acid residues such as SER-378, LYS-366, ARG-375, ARG-407, LYS-412 were highlighted. It revealed that atracurium besilate can dock well to EGR1. (b) The binding mode of methotrexate to the EGR1 was analyzed, in which some carboxyl active groups such as ASP-381, HIS-382, ARG-375, ARG-407 were displayed. It also suggested that methotrexate can dock well to EGR1. (A color version of this figure is available in the online journal.)

Discussion

The underlying mechanism of therapy resistance to enzalutamide in CRPC has not been fully elucidated thus far. In recently existing studies, the aberrant reactivation of AR signaling has been an emphasis through several mechanisms involving AR mutations,¹² AR amplifications¹³ and AR splicing variants.¹⁴ Meanwhile, AR alternative signaling pathways, which are also known as “AR bypass pathways”, remain a pivotal driver in mediating disease

progression in CRPC through CXCR7-VEGF-VEGFR2¹¹, HER2-YB1-AR,¹⁵ PI3K-AKT-mTOR,¹⁶ NF- κ B/P52,¹⁷ and TGF- β 1/STAT3¹⁸ signaling. Of note, PCa initially presents as an androgen-sensitive state, and then progresses to an androgen-independent state, but eventually evolves into CRPC. During this process, for the AR signaling pathway or for alternative signaling pathways, no matter inactivation of the former or the activation of the latter will cause enzalutamide-resistance essentially. Hence, to gain a

deeper insight into its molecular mechanisms, the enzalutamide-resistant cell model must meet two conditions: (1) Inhibition of AR signaling activity to the greatest extent. (2) AR alternative signaling pathways were fully activated as much as possible.

Currently, two main cell models were employed to simulate CRPC phase at home and abroad. The first one is that androgen-independent cell lines directly substitute for castration resistant model to perform subsequent researches. Another model is that androgen-independent cell strains, such as DU-145, CWR22Rv1, C4-2B and PC-3, which were both derived from castrated mice cultivated *in vitro*, or androgen-dependent cell strains received some time treatment with the reagent above mentioned was carried out to simulate clinical CRPC status.

Previous studies have shown that the overexpression of metastasis tumor suppressor-1 (MTSS-1) in PC-3 cells attenuated cell migration, growth, and adherence properties, whereas MTSS-1 knockdown in DU-145 cells can promote the above abilities.¹⁹ In LNCaP and 22Rv1 cells, melatonin can inhibit the gene transcription and AR-V7/NF- κ B pathway activation, thereby further delaying the progression of PCa by disrupting their interaction with each other positively.²⁰ Meanwhile, to find a model to mimic the CRPC status, 22Rv1 cells with high AKR1C3 expression were performed to carry out the subsequent experiments by Tian *et al.*²¹ They observed that berberine can reduce androgen synthesis with the help of the inhibitor, Aldo-keto reductase family 1 member C3 (AKR1C3), resulting in delaying the progression of CRPC. Taken together, only partial AR pathway activity was attenuated, whereas AR alternative pathway activity was not fully activated to a certain extent in the above cell models. Secondly, the above cells still showed drug responses to enzalutamide, which is not completely understood as enzalutamide-resistant CRPC.

The establishment of another enzalutamide-resistant cell models was mostly based on enzalutamide combined with some antagonist treatment such as AR, Jagged1-Notch1, CXCR4, CXCR7, EGFR, JAK, STAT, C-Myc for a period of time. To generate enzalutamide-resistant cells, the LNCaP cells were given 10- μ M enzalutamide for at least six months in Luo *et al.* studies.^{22,23} Similar to Luo *et al.* cell model, in the related model, to assess AZD5363's effects, some researchers gave MR49C and MR49F cells with enzalutamide to gain enzalutamide resistance.²⁴ Additional study corroborated that niclosamide played a positive role in inhibiting AR variation and enzalutamide-resistance in CRPC based on C4-2B MR cell models,²⁵ which was derived from C4-2B cells chronically exposed to increasing concentrations of enzalutamide (ranging from 5–40 μ M) more than one year. Scott *et al.* in 2013 confirmed that AR shear variant AR-v7 was the first drug-resistant gene in the enzalutamide-resistant CRPC experimental model, which was derived from CWR22-R1 cells treated with 1 μ M enzalutamide for long-term.²⁶ In our previous study,¹¹ by giving VCaP and C4-2B with enzalutamide (1 μ M) for one day to construct CRPC models, it was demonstrated that the combination treatment of enzalutamide and CCX771 (CXCR7 inhibitor) can inhibit cell growth and angiogenesis. Altogether, the inhibition of AR signaling activity and the

activation of AR alternative signaling activity in such cell models were both further enhanced compared to the first cell model. However, the above cell models simulated the process of androgen-independent progress to androgen resistance stage and cannot be completely considered as enzalutamide-resistant cell model.

In summary, in this study, we constructed an enzalutamide-resistant cell model based on the above two cell models and validated its drug resistance in several *in vitro* and *in vivo* experiments. Furthermore, we also screened some functional resistance genes involved in the development of enzalutamide-resistance and small molecular drugs concerned with the amelioration of enzalutamide-resistance. Of clinical relevance, EGR1 may serve as a potential diagnostic marker for enzalutamide-resistant CRPC, and by targeting EGR1, CRPC may be treated potentially in a new way. In addition, validation of our data is certainly guaranteed among different CRPC sufferers largely.

AUTHORS' CONTRIBUTIONS

All authors participated in the design of experiment, therein, FT wrote the manuscript and WDC conducted the experiment, all participated in data analysis and manuscript reading, review, and finalizing, LY was responsible for the final version of the article.

DECLARATION OF CONFLICTING INTERESTS

The author(s) declared no potential conflicts of interest with respect to the research, authorship, and/or publication of this article.

FUNDING

The author(s) disclosed receipt of the following financial support for the research, authorship, and/or publication of this article: This work was supported by The Natural Science Foundation of Beijing (grant number 7172068 and 7192053).

ORCID iD

Tao Feng  <https://orcid.org/0000-0002-4498-5118>

REFERENCES

1. Ferlay J, Soerjomataram I, Dikshit R, Eser S, Mathers C, Rebelo M, Parkin DM, Forman D, Bray F. Cancer incidence and mortality worldwide: sources, methods and major patterns in GLOBOCAN 2012. *Int J Cancer* 2015;**136**:E359–86
2. Tilki D, Schaeffer EM, Evans CP. Understanding mechanisms of resistance in metastatic castration-resistant prostate cancer: the role of the androgen receptor. *Eur Urol Focus* 2016;**2**:499–505
3. Rini BI, Small EJ. Hormone-refractory prostate cancer. *Curr Treat Options Oncol* 2002;**3**:437–46
4. Beer TM, Armstrong AJ, Rathkopf DE, Loriot Y, Sternberg CN, Higano CS, Iversen P, Bhattacharya S, Carles J, Chowdhury S, Davis ID, de Bono JS, Evans CP, Fizazi K, Joshua AM, Kim CS, Kimura G, Mainwaring P, Mansbach H, Miller K, Noonberg SB, Perabo F, Phung D, Saad F, Scher HI, Taplin ME, Venner PM, Tombal B, Investigators P. Enzalutamide in metastatic prostate cancer before chemotherapy. *N Engl J Med* 2014;**371**:424–33

5. Scher HI, Cabot RC, Harris NL, Rosenberg ES, Shepard J-AO, Cort AM, Ebeling SH, McDonald EK, Fizazi K, Saad F, Taplin M-E, Sternberg CN, Miller K, de Wit R, Mulders P, Chi KN, Shore ND, Armstrong AJ, Flaig TW, Fléchon A, Mainwaring P, Fleming M, Hainsworth JD, Hirmand M, Selby B, Seely L, de Bono JS. Increased survival with enzalutamide in prostate cancer after chemotherapy. *N Engl J Med* 2012;**367**:1187–97
6. Beer TM, Armstrong AJ, Rathkopf D, Loriot Y, Sternberg CN, Higano CS, Iversen P, Evans CP, Kim C-S, Kimura G, Miller K, Saad F, Bjartell AS, Borre M, Mulders P, Tammela TL, Parli T, Sari S, van Os S, Theeuwes A, Tombal B. Enzalutamide in men with chemotherapy-naïve metastatic castration-resistant prostate cancer: extended analysis of the phase 3 PREVAIL study. *Eur Urol* 2017;**71**:151–4
7. Maughan BL, Lubner B, Nadal R, Antonarakis ES. Comparing sequencing of abiraterone and enzalutamide in men with metastatic castration-resistant prostate cancer: a retrospective study. *Prostate* 2017;**77**:33–40
8. Tannock IF, de Wit R, Berry WR, Horti J, Pluzanska A, Chi KN, Oudard S, Théodore C, James ND, Turesson I, Rosenthal MA, Eisenberger MA. Docetaxel plus prednisone or mitoxantrone plus prednisone for advanced prostate cancer. *N Engl J Med* 2004;**351**:1502–12
9. Subramanian A, Narayan R, Corsello SM, Peck DD, Natoli TE, Lu X, Gould J, Davis JF, Tubelli AA, Asiedu JK, Lahr DL, Hirschman JE, Liu Z, Donahue M, Julian B, Khan M, Wadden D, Smith IC, Lam D, Liberzon A, Toder C, Bagul M, Orzechowski M, Enache OM, Piccioni F, Johnson SA, Lyons NJ, Berger AH, Shamji AF, Brooks AN, Vrcic A, Flynn C, Rosains J, Takeda DY, Hu R, Davison D, Lamb J, Ardlie K, Hogstrom L, Greenside P, Gray NS, Clemons PA, Silver S, Wu X, Zhao WN, Read-Button W, Wu X, Haggarty SJ, Ronco LV, Boehm JS, Schreiber SL, Doench JG, Bittker JA, Root DE, Wong B, Golub TR. A next generation connectivity map: L1000 platform and the first 1,000,000 profiles. *Cell* 2017;**171**:1437–52.e17
10. Lamb J, Crawford ED, Peck D, Modell JW, Blat IC, Wrobel MJ, Lerner J, Brunet JP, Subramanian A, Ross KN, Reich M, Hieronymus H, Wei G, Armstrong SA, Haggarty SJ, Clemons PA, Wei R, Carr SA, Lander ES, Golub TR. The connectivity map: using gene-expression signatures to connect small molecules, genes, and disease. *Science* 2006;**313**:1929–35
11. Luo Y, Azad AK, Karanika S, Basourakos SP, Zuo X, Wang J, Yang L, Yang G, Korentzelos D, Yin J, Park S, Zhang P, Campbell JJ, Schall TJ, Cao G, Li L, Thompson TC. Enzalutamide and CXCR7 inhibitor combination treatment suppresses cell growth and angiogenic signaling in castration-resistant prostate cancer models. *Int J Cancer* 2018;**142**:2163–74
12. Azad AA, Volik SV, Wyatt AW, Haegert A, Le Bihan S, Bell RH, Anderson SA, McConeghy B, Shukin R, Bazov J, Youngren J, Paris P, Thomas G, Small EJ, Wang Y, Gleave ME, Collins CC, Chi KN. Androgen receptor gene aberrations in circulating cell-free DNA: biomarkers of therapeutic resistance in castration-resistant prostate cancer. *Clin Cancer Res* 2015;**21**:2315–24
13. Yuan X, Balk SP. Mechanisms mediating androgen receptor reactivation after castration. *Urol Oncol* 2009;**27**:36–41
14. Luo J, Attard G, Balk SP, Bevan C, Burnstein K, Cato L, Cherkasov A, De Bono JS, Dong Y, Gao AC, Gleave M, Heemers H, Kanayama M, Kittler R, Lang JM, Lee RJ, Logothetis CJ, Matusik R, Plymate S, Sawyers CL, Selth LA, Soule H, Tilley W, Weigel NL, Zoubeidi A, Dehm SM, Raj GV. Role of androgen receptor variants in prostate cancer: report from the 2017 mission androgen receptor variants meeting. *Eur Urol* 2018;**73**:715–23
15. Shiota M, Bishop JL, Takeuchi A, Nip KM, Cordonnier T, Beraldi E, Kuruma H, Gleave ME, Zoubeidi A. Inhibition of the HER2-YB1-AR axis with lapatinib synergistically enhances enzalutamide anti-tumor efficacy in castration resistant prostate cancer. *Oncotarget* 2015;**6**:9086–98
16. He C, Duan S, Dong L, Wang Y, Hu Q, Liu C, Forrest ML, Holzbeierlein JM, Han S, Li B. Characterization of a novel p110beta-specific inhibitor BL140 that overcomes MDV3100-resistance in castration-resistant prostate cancer cells. *Prostate* 2017;**77**:1187–98
17. Nadiminty N, Tummala R, Liu C, Yang J, Lou W, Evans CP, Gao AC. NF-kappaB2/p52 induces resistance to enzalutamide in prostate cancer: role of androgen receptor and its variants. *Mol Cancer Ther* 2013;**12**:1629–37
18. Liu Q, Tong D, Liu G, Xu J, Do K, Geary K, Zhang D, Zhang J, Zhang Y, Li Y, Bi G, Lan W, Jiang J. Metformin reverses prostate cancer resistance to enzalutamide by targeting TGF-β1/STAT3 axis-regulated EMT. *Cell Death Dis* 2017;**8**:e3007
19. Mustafa N, Martin TA, Jiang WG. Metastasis tumour suppressor-1 and the aggressiveness of prostate cancer cells. *Exp Ther Med* 2011;**2**:157–62
20. Liu V, Yau W, Tam C, Yao K-M, Shiu S. Melatonin inhibits androgen receptor splice variant-7 (AR-V7)-induced nuclear Factor-Kappa B (NF-κB) activation and NF-κB Activator-Induced AR-V7 expression in prostate cancer cells: potential implications for the use of melatonin in castration-resistant prostate cancer (CRPC) therapy. *Int J Mol Sci* 2017;**18**:1130
21. Li J, Tian Y, Zhao L, Wang Y, Zhang H, Xu D, Zhao X, LY. Berberine inhibits androgen synthesis by interaction with aldo-keto reductase 1C3 in 22Rv1 prostate cancer cells. *Asian J Androl* 2016;**18**:607–12
22. Sun W, Li L, Du Z, Quan Z, Yuan M, Cheng H, Gao Y, Luo C, Wu X. Combination of phospholipase epsilon knockdown with GANT61 sensitizes castration-resistant prostate cancer cells to enzalutamide by suppressing the androgen receptor signaling pathway. *Oncol Rep* 2019;**41**:2689–702
23. Du Z, Li L, Sun W, Wang X, Zhang Y, Chen Z, Yuan M, Quan Z, Liu N, Hao Y, Li T, Wang J, Luo C, Wu X. HepaCAM inhibits the malignant behavior of castration-resistant prostate cancer cells by downregulating notch signaling and PF-3084014 (a γ-secretase inhibitor) partly reverses the resistance of refractory prostate cancer to docetaxel and enzalutamide in vitro. *Int J Oncol* 2018;**53**:99–112
24. Kuruma H, Matsumoto H, Shiota M, Bishop J, Lamoureux F, Thomas C, Briere D, Los G, Gleave M, Fanjul A, Zoubeidi A. A novel antiandrogen, compound 30, suppresses castration-resistant and MDV3100-Resistant prostate cancer growth in vitro and in vivo. *Mol Cancer Ther* 2013;**12**:567–76
25. Liu C, Lou W, Zhu Y, Nadiminty N, Schwartz CT, Evans CP, Gao AC. Niclosamide inhibits androgen receptor variants expression and overcomes enzalutamide resistance in castration-resistant prostate cancer. *Clin Cancer Res* 2014;**20**:3198–210
26. Li Y, Chan SC, Brand LJ, Hwang TH, Silverstein KAT, Dehm SM. Androgen receptor splice variants mediate enzalutamide resistance in castration-resistant prostate cancer cell lines. *Cancer Res* 2013;**73**:483–9

(Received January 17, 2021, Accepted April 2, 2021)